JOC Article

Reaction Mechanism and Stereoselectivity of Ruthenium−Porphyrin-Catalyzed Intramolecular Amidation of Sulfamate Ester: A DFT Computational Study

Xufeng Lin, Chi-Ming Che,* and David Lee Phillips*

Department of Chemistry and Open Laboratory of Chemical Biology of the Institute of Molecular Technology for Drug Discovery and Synthesis, The University of Hong Kong, Pokfulam Road, Hong Kong, P.R. 11111, China

cmche@hku.hk; phillips@hkucc.hku.hk

Received September 13, 2007

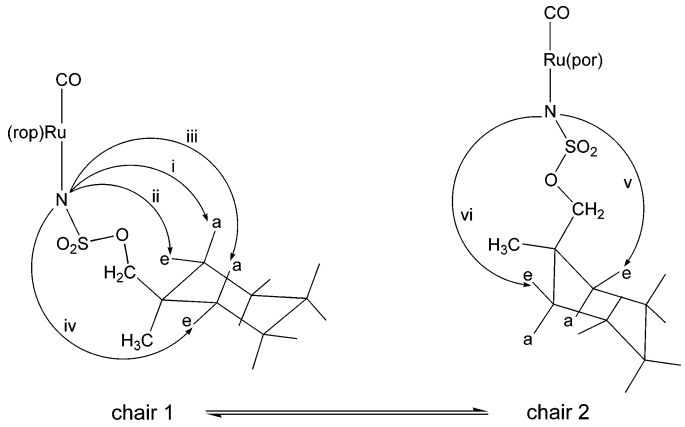

The reaction mechanism of the ruthenium−porhyrin complex [Ru(por)(CO)]-catalyzed intramolecular C−H bond amidation was examined using density functional theory (DFT) calculations. The metal−nitrene reactive intermediate, Ru(por)(CO)−NSO_3R^1 (R^1 = 1-methylclohexl-methyl) was found to be highly favorable to generate in terms of the free energy profile from the reaction of the starting materials. Ru(por)(CO)−NSO_3R^1 may exist in both singlet and triplet states since they are close in energy. In each state, six C−H bond amidation reaction pathways were characterized structurally and energetically. The predicted most probable diastereomeric product out of the four possible diasteromeric products examined in the calculations for the amidation reactions agree well with previously reported experimental results.

1. Introduction

Transition metal complexes catalyzed the amidation of C−H bonds are increasingly attractive as a synthetic route to functional amides and amines.[1−15] An important step for these types of catalytic processes is the delivery of a nitrene moiety by a metal ion into a C−H bond, and iminoiodanes (PhI═NY, Y = -SO_2R, -SO_3R, -COOR, -Ts...), PhI$(OAc)_2$ + H_2N−Y, or PhIO + H_2N−Y are often used as a nitrene source for the generation of reactive metal−nitrene (M═NY) intermediates that have generally been proposed to be involved in these reactions. However, the actual reactive intermediate(s) directly responsible for the nitrene insertion into the C−H bonds remains elusive in the literature. To better understand the chemistry of C−H bond functionalization via C−N bond formation, we envision that it is indispensible to perform a computational study to help elucidate the processes taking place in metal-catalyzed C−H bond amidations. In the literature, computational studies on metal-catalyzed nitrene transfer to C═C double bonds and insertion into C−H bonds are sparse,[6d,16] although there is increasing interest in using transition metal complexes for the

* Corresponding author. Fax: 852-2857-1586.

(1) (a) Breslow, R.; Gellman, S. H. *J. Chem. Soc., Chem. Commun.* **1982**, 1400. (b) Breslow, R.; Gellman, S. H. *J. Am. Chem. Soc.* **1983**, *105*, 6728. (c) Yang, J.; Weinberg, R.; Breslow, R. *Chem. Commun.* **2000**, 531.

(2) (a) Mansuy, D.; Mahy, J.-P.; Dureault, A.; Bedi, G.; Battioni, G. *J. Chem. Soc., Chem. Commun.* **1984**, 1161. (b) Mahy, J.-P.; Battioni, P.; Mansuy, D. *J. Am. Chem. Soc.* **1986**, *108*, 1079. (c) Mahy, J.-P.; Bedi, G.; Battioni, P.; Mansuy, D. *J. Chem. Soc., Perkin Trans. 2* **1988**, 1517. (d) Mahy, J.-P.; Bedi, G.; Battioni, P.; Mansuy, D. *New. J. Chem.* **1989**, *13*, 651.

(3) (a) Evans, D. A.; Faul, M. M.; Bilodeau, M. T. *J. Org. Chem.* **1991**, *56*, 6744. (b) Evans, D. A.; Faul, M. M.; Bilodeau, M. T.; Anderson, B. A.; Barnes, D. M. *J. Am. Chem. Soc.* **1993**, *115*, 5328. (c) Evans, D. A.; Faul, M. M.; Bilodeau, M. T. *J. Am. Chem. Soc.* **1994**, *116*, 2742.

10.1021/jo702011z CCC: $40.75
Published on Web 12/20/2007

amidation of C−H bonds for applications in synthetic chemistry. Recently, a number of transition metals having diverse ligand scaffolds and tunable electronic properties has been developed to become useful catalysts for producing regio- or stereoselective amidation products.[8g,h,l,9a] It would be of great interest to seek rationales that govern the selectivity of metal-catalyzed nitrene trnasfer reactions with theoretical calculations so as to aid the design of new catalysts.

To gain insight into the reaction mechanism of C−H bond amidation, as well as an explanation/prediction for the stereoselectivity of these types of reactions, a computational study was performed in this work on the reaction depicted in Scheme 1, which is the intramolecular amidation of a C−H bond of a cyclohexyl ring to form a diastereoselective amide with two asymmetric C centers.[8g] The catalyst of this reaction is Ru(F_{20}-TPP)(CO) [**4a**, where F_{20}-TPP = tetra(pentafluorophenyl)-porphyrin], which was modeled by Ru(por)(CO) and denoted as **4b** in Scheme 1. The formation of a six-membered ring amide requires the nitrogen atom to be inserted into one of the C−H bonds at the $C^{(6)}$ or $C^{(7)}$ sites, each of which has two C−H bonds. Amidation of these four C−H bonds will lead to different diastereomers; however, only one diastereomer (5*R*, 6*S*) of the six-membered ring amide **3** was found as the reaction product in experiments.

SCHEME 1. Ru(F_{20}-TPP)(CO)-Catalyzed C−N Bond Formation of a Sulfamate Ester[a]

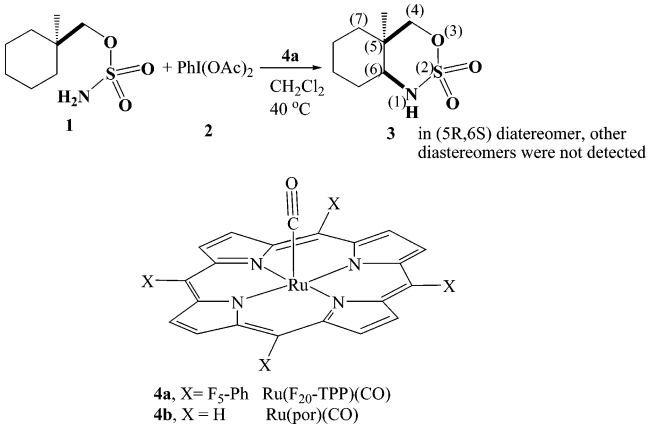

[a] See Table 1, entry 6 in ref 8g.

Previously, we reported a density functional theory (DFT) study on dirhodium tetracarboxylate [$Rh_2(O_2CH)_4$]-catalyzed C−N bond formation reactions.[16] $Rh_2(O_2CH)_4$−NCOOR′ (R′ = 2-methylbutyl) was found to be favorable with a free energy much lower (∼12 kcal/mol) than that of $Rh_2(O_2CH)_4$−N(PhI)−COOR′. Taking into account the controversy as to whether a metal−iminoiodane [L_xM−N(IPh)−Y] or a metal−nitrene [L_xM−NY] is directly responsible for the delivery of the nitrene moeity,[1,2,4,8,15a] we also examined the energy and free energy profiles for the generation of a Ru(por)(CO)−nitrene **7** species from the starting materials (see Scheme 2) in this work. Since it is well-known that iminoiodane **5** can be in situ generated from $PhI(OAc)_2$ **2** and sulfamate **1** with the release of an acetic acid,[8,9] the starting materials can actually be the catalyst Ru(por)(CO) and PhI=NSO_3R^1, where R^1 = 1-methylclohexl-

(4) (a) Müller, P.; Baud, C.; Jacquier, Y.; Moran, M.; Nägeli, I. *J. Phys. Org. Chem.* **1996**, *9*, 341. (b) Müller, P.; Baud, C.; Jacquier, Y. *Tetrahedron* **1996**, *52*, 1543. (c) Nägeli, I.; Baud, C.; Bernardinelli, G.; Jacquier, Y.; Moran, M.; Müller, P. *Helv. Chim. Acta* **1997**, *80*, 1087. (d) Müller, P.; Baud, C.; Nägeli, I. *J. Phys. Org. Chem.* **1998**, *11*, 597. (e) Müller, P.; Baud, C.; Jacquier, Y. *Can. J. Chem.* **1998**, *76*, 738. (f) Müller, P.; Fruit, C. *Chem. Rev.* **2003**, *103*, 2905. (g) Fruit, C.; Müller, P. *Tetrahedron: Asymmetry* **2004**, *15*, 1019. (h) Fruit, C.; Müller, P. *Helv. Chim. Acta* **2004**, *87*, 1607.

(5) (a) Nishikori, H.; Katsuki, T. *Tetrahedron Lett.* **1996**, *37*, 9245. (b) Kohmura, Y.; Katsuki, T. *Tetrahedron Lett.* **2001**, *42*, 3339.

(6) (a) Södergren, M. J.; Alonso, D. A.; Andersson, P. G. *Tetrahedron: Asymmetry* **1997**, *8*, 3563. (b) Södergren, M. J.; Alonso, D. A.; Bedekar, A. V.; Andersson, P. G. *Tetrahedron Lett.* **1997**, *38*, 6897. (c) Bertilsson, S. K.; Tedenborg, L.; Alonso, D. A.; Andersson, P. G. *Organometallics* **1999**, *18*, 1281. (d) Brandt, P.; Södergren, M. J.; Andersson, P. G.; Norrby, P.-O. *J. Am. Chem. Soc.* **2000**, *122*, 8013.

(7) (a) Díaz-Requejo, M. M.; Pérez, P. J.; Brookhart, M.; Templeton, J. L. *Organometallics* **1997**, *16*, 4399. (b) Díaz-Requejo, M. M.; Belderraín, T. R.; Nicasio, M. C.; Trofimenko, S.; Pérez, P. J. *J. Am. Chem. Soc.* **2003**, *125*, 12078. (c) Mairena, M. A.; Díaz-Requejo, M. M.; Belderraín, T. R.; Nicasio, M. C.; Trofimenko, S.; Pérez, P. J. *Organometallics* **2004**, *23*, 253.

(8) (a) Lai, T.-S.; Kwong, H.-L.; Che, C.-M.; Peng, S.-M. *Chem. Commun.* **1997**, 2373. (b) Au, S.-M.; Zhang, S.-B.; Fung, W.-H.; Yu, W.-Y.; Che, C.-M.; Cheung, K.-K. *Chem. Commun.* **1998**, 2677. (c) Zhou, X.-G.; Yu, X.-Q.; Huang, J.-S.; Che, C.-M. *Chem. Commun.* **1999**, 2377. (d) Yu, X.-Q.; Huang, J.-S.; Zhou, X.-G.; Che, C.-M. *Org. Lett.* **2000**, *2*, 2233. (e) Au, S.-M.; Huang, J.-S.; Che, C.-M.; Yu, W.-Y. *J. Org. Chem.* **2000**, *65*, 7858. (f) Liang, J.-L.; Huang, J.-S.; Yu, X.-Q.; Zhu, N.; Che, C.-M. *Chem.*−*Eur. J.* **2002**, *8*, 1563. (g) Liang, J.-L.; Yuan, S.-X.; Huang, J.-S.; Yu, W.-Y.; Che, C.-M. *Angew. Chem., Int. Ed.* **2002**, *41*, 3465. (h) Liang, J.-L.; Yuan, S.-X.; Chan, P. W. H.; Che, C.-M. *Org. Lett.* **2002**, *4*, 4507. (i) Liang, J.-L.; Yuan, S.-X.; Chan, P. W. H.; Che, C.-M. *Tetrahedron Lett.* **2003**, *44*, 5917. (j) Liang, J.-L.; Yuan, S.-X.; Huang, J.-S.; Che, C.-M. *J. Org. Chem.* **2004**, *69*, 3610. (k) He, L.; Chan, P. W. H.; Tsui, W.-M.; Yu, W.-Y.; Che, C.-M. *Org. Lett.* **2004**, *6*, 2405. (l) Leung, S. K.-Y.; Tsui, W.-M.; Huang, J.-S.; Che, C.-M.; Liang, J.-L.; Zhu, N. *J. Am. Chem. Soc.* **2005**, *127*, 16629.

(9) (a) Espino, C. G.; Du Bois, J. *Angew. Chem., Int. Ed.* **2001**, *40*, 598. (b) Espino, C. G.; Wehn, P. M.; Chow, J.; Du Bois, J. *J. Am. Chem. Soc.* **2001**, *123*, 6935. (c) Guthikonda, K.; Du Bois, J. *J. Am. Chem. Soc.* **2002**, *124*, 13672. (d) Fleming, J. J.; Fiori, K. W.; Du Bois, J. *J. Am. Chem. Soc.* **2003**, *125*, 2028. (e) Wehn, P. M.; Lee, J.; Du Bois, J. *Org. Lett.* **2003**, *5*, 4823. (f) Espino, C. G.; Fiori, K. W.; Kim, M.; Du Bois, J. *J. Am. Chem. Soc.* **2004**, *126*, 15378. (g) Fiori, K. W.; Fleming, J. J.; Du Bois, J. *Angew. Chem., Int. Ed.* **2004**, *43*, 4349.

(10) (a) Dauban, P.; Dodd, R. H. *Tetrahedron Lett.* **1998**, *39*, 5739. (b) Dauban, P.; Dodd, R. H. *J. Org. Chem.* **1999**, *64*, 5304. (c) Dauban, P.; Dodd, R. H. *Org. Lett.* **2000**, *2*, 2327. (d) Dauban, P.; Sanière, L.; Tarrade, A.; Dodd, R. H. *J. Am. Chem. Soc.* **2001**, *123*, 7707. (e) Duran, F.; Leman, L.; Ghini, A.; Burton, G.; Dauban, P.; Dodd, R. H. *Org. Lett.* **2002**, *4*, 2481. (f) Dauban, P.; Dodd, R. H. *Synlett* **2003**, 1571. (g) Sanière, L.; Leman, L.; Bourguignon, J.-J.; Dauban, P.; Dodd, R. H. *Tetrahedron* **2004**, *60*, 5889.

(11) (a) Halfen, J. A.; Hallman, J. K.; Schultz, J. A.; Emerson, J. P. *Organometallics* **1999**, *18*, 5435. (b) Halfen, J. A.; Uhan, J. M.; Fox, D. C.; Mehn, M. P.; Que, L., Jr. *Inorg. Chem.* **2000**, *39*, 4913. (c) Halfen, J. A.; Fox, D. C.; Mehn, M. P.; Que, L., Jr. *Inorg. Chem.* **2001**, *40*, 5060.

(12) (a) Sanders, C. J.; Gillespie, K. M.; Bell, D.; Scott, P. *J. Am. Chem. Soc.* **2000**, *122*, 7132. (b) Gillespie, K. M.; Crust, E. J.; Deeth, R. J.; Scott, P. *Chem. Commun.* **2001**, 785. (c) Gillespie, K. M.; Sanders, C. J.; O'Shaughnessy, P.; Westmoreland, I.; Thickitt, C. P.; Scott, P. *J. Org. Chem.* **2002**, *67*, 3450.

(13) (a) Padwa, A.; Stengel, T. *Org. Lett.* **2002**, *4*, 2137. (b) Padwa, A.; Flick, A. C.; Leverett, C. A.; Stengel, T. *J. Org. Chem.* **2004**, *69*, 6377.

(14) (a) Cui, Y.; He, C. *J. Am. Chem. Soc.* **2003**, *125*, 16202. (b) Cui, Y.; He, C. *Angew. Chem., Int. Ed.* **2004**, *43*, 4210.

(15) (a) Li, Z.; Quan, R. W.; Jacobsen, E. N. *J. Am. Chem. Soc.* **1995**, *117*, 5889. (b) Harm, A. M.; Knight, J. G.; Stemp, G. *Tetrahedron Lett.* **1996**, *37*, 6189. (c) Adam, W.; Roschmann, K. J.; Saha-Möller, C. R. *Eur. J. Org. Chem.* **2000**, 557. (d) Llewellyn, D. B.; Adamson, D.; Arndtsen, B. A. *Org. Lett.* **2000**, *2*, 4165. (e) Taylor, S.; Gullick, J.; McMorn, P.; Bethell, D.; Page, P. C. B.; Hancock, F. E.; King, F.; Hutchings, G. J. *J. Chem. Soc., Perkin Trans. 2* **2001**, 1714. (f) Comba, P.; Merz, M.; Pritzkow, H. *Eur. J. Inorg. Chem.* **2003**, 1711. (g) Avenier, F.; Latour, J.-M. *Chem. Commun.* **2004**, 1544. (h) Xu, J.; Ma, L.; Jiao, P. *Chem. Commun.* **2004**, 1616. (i) Leca, D.; Toussaint, A.; Mareau, C.; Fensterbank, L.; Lacôte, E.; Malacria, M. *Org. Lett.* **2004**, *6*, 3573. (j) Han, H.; Bae, I.; Yoo, E. J.; Lee, J.; Do, Y.; Chang, S. *Org. Lett.* **2004**, *6*, 4109. (k) Amisial, L. D.; Dai, X.; Kinney, R. A.; Krishnaswamy, A.; Warren, T. H. *Inorg. Chem.* **2004**, *43*, 6537.

(16) Lin, X.; Zhao, C.; Che, C. M.; Ke, Z.; Phillips, D. L. *Chem. Asian J.* **2007**, *2*, 1101.

SCHEME 2. Catalytic Cycle of Ru-Catalyzed Intramolecular Amidation of C−H Bonds Characterized in This Work[a]

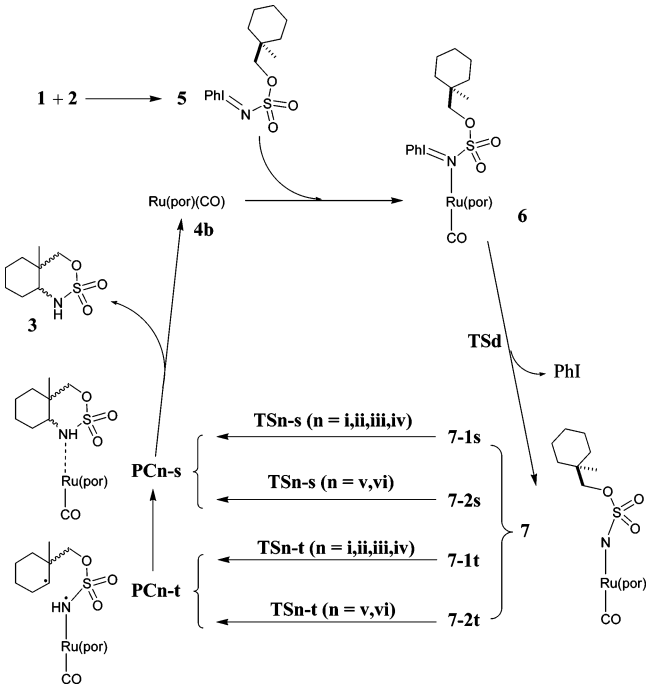

[a] R^1 = 1-methylclohexl-methyl. Ru(por)(CO) was used to model (F_{20}-TPP)(CO) in Scheme 1.

methyl (i.e., SM = **4b** + **5**). In ref 16, it was found that the C−H bond amidation step via the metal−nitrene complex can undergo several different pathways and that the relative reaction rates of these pathways determine the selectivity of the final amidation product. In this study, we examined the free energy profiles of the twelve possible reaction pathways for producing the six-membered ring amide **3**. The production of **3** was accompanied by the regeneration of catalyst **4b**, so that the whole catalytic cycle examined here can be depicted as displayed in Scheme 2. From the results of the C−H bond amidation step (**7** → **3** + **4b**), the predicted diastereomeric product out of four possible diasteoromers agrees well with previously reported experimental results.[8g]

2. Computational Methods

The potential energy surfaces (PES) of the Ru-catalyzed C−H bond amidation reactions were investigated by locating the structures with the energy minimum (for reactants, reactant complexes, and product complexes) and the first-order saddle point (for transition states) involved in the catalytic cycle indicated in Scheme 2. To save computational resources, we used Ru(por)(CO) **4b** to model Ru(F_{20}-TPP)(CO) **4a** found in the real reaction systems. Geometry optimization and frequency analysis were performed using DFT with the Gaussian 98 suite of programs (A7 version).[17a] Becke's 1988 exchange in conjunction with the PW91 correlation fucntionals[18] were used for the DFT calculations, and three basis set levels (denoted as BS1 to ~BS3) were compared in benchmark calculations (see sections 3.2. and 3.3. for details). In all three basis sets, SDD was used for the Ru atom,[19] and LANL2DZ in conjunction with a 0.266 d polarization was used for the I atom.[20] In BS1, the 6-31G basis set was used for all of the C, H, and O atoms, and the 6-31G* basis set was used for the N and S atoms. In BS2, 6-31G* was employed for all of the C, H, O, N, and S atoms. In BS3, the 6-311G** basis set was used for all of the C, H, O, N, and S atoms. As this reaction was experimentally carried out in a CH_2Cl_2 solvent, bulk solvation effects were also examined in performing the calculations with the polarized continuum model (D-PCM)[21] (implemented in the latest version of Gaussian 03)[17b] utilized for CH_2Cl_2 (ϵ = 8.30 at 313.15 K). Bondi's atomic radii[22] were used in the PCM calculations, in which the hydrogen atoms were explicitly considered to build up the solvation cavity. Intrinsic reaction coordinate (IRC) calculations were performed to confirm the transition states connected to the appropriate reactants and products.[23] The Cartesian coordinates, total energies, and vibrational zero-point energies (ZPE) for the computed structures are given in the Supporting Information. The energy data in the following text are ZPE corrected energies except those listed in Table 1.

TABLE 1. BPW91 Computed E_{st} ($E_{7-1s} - E_{7-1t}$) of the Ruthenium−Nitrene Complex 7-1 with Different Basis Set Levels and with Consideration of Solvation Effects in the DPCM Model[a]

method	E_{ST}	$\Delta E^{\ddagger}_{i-s}$
BPW91/BS1	−0.5	22.9
D-PCM//BPw91/BS1	0.0	20.3
BPW91/BS2	−1.2	23.1
D-PCM//BPW91/BS2	−0.7	21.3
BPW91/BS3//BPW91/BS2	−0.6	21.1

[a] ZPE corrections were not included.

3. Results and Discussion

3.1. Generation of the Ru(por)(CO)−Nitrene Complex from the Starting Materials (4b + 5). The BPW91/BS1

(17) (a) Frisch, M. J.; Trucks, G. W.; Schlegel, H. B.; Scuseria, G. E.; Robb, M. A.; Cheeseman, J. R.; Zakrzewski, V. G.; Montgomery, J. A., Jr.; Stratmann, R. E.; Burant, J. C.; Dapprich, S.; Millam, J. M.; Daniels, A. D.; Kudin, K. N.; Strain, M. C.; Farkas, O.; Tomasi, J.; Barone, V.; Cossi, M.; Cammi, R.; Mennucci, B.; Pomelli, C.; Adamo, C.; Clifford, S.; Ochterski, J.; Petersson, G. A.; Ayala, P. Y.; Cui, Q.; Morokuma, K.; Rega, N.; Salvador, P.; Dannenberg, J. J.; Malick, D. K.; Rabuck, A. D.; Raghavachari, K.; Foresman, J. B.; Cioslowski, J.; Ortiz, J. V.; Baboul, A. G.; Stefanov, B. B.; Liu, G.; Liashenko, A.; Piskorz, P.; Komaromi, I.; Gomperts, R.; Martin, R. L.; Fox, D. J.; Keith, T.; Al-Laham, M. A.; Peng, C. Y.; Nanayakkara, A.; Challacombe, M.; Gill, P. M. W.; Johnson, B.; Chen, W.; Wong, M. W.; Andres, J. L.; Gonzalez, C.; Head-Gordon, M.; Replogle, E. S.; Pople, J. A. *Gaussian 98*, Revision A.11.3; Gaussian, Inc.: Pittsburgh, PA, 2002. (b) Frisch, M. J.; Trucks, G. W.; Schlegel, H. B.; Scuseria, G. E.; Robb, M. A.; Cheeseman, J. R.; Montgomery, J. A., Jr.; Vreven, T.; Kudin, K. N.; Burant, J. C.; Millam, J. M.; Iyengar, S. S.; Tomasi, J.; Barone, V.; Mennucci, B.; Cossi, M.; Scalmani, G.; Rega, N.; Petersson, G. A.; Nakatsuji, H.; Hada, M.; Ehara, M.; Toyota, K.; Fukuda, R.; Hasegawa, J.; Ishida, M.; Nakajima, T.; Honda, Y.; Kitao, O.; Nakai, H.; Klene, M.; Li, X.; Knox, J. E.; Hratchian, H. P.; Cross, J. B.; Adamo, C.; Jaramillo, J.; Gomperts, R.; Stratmann, R. E.; Yazyev, O.; Austin, A. J.; Cammi, R.; Pomelli, C.; Ochterski, J. W.; Ayala, P. Y.; Morokuma, K.; Voth, G. A.; Salvador, P.; Dannenberg, J. J.; Zakrzewski, V. G.; Dapprich, S.; Daniels, A. D.; Strain, M. C.; Farkas, O.; Malick, D. K.; Rabuck, A. D.; Raghavachari, K.; Foresman, J. B.; Ortiz, J. V.; Cui, Q.; Baboul, A. G.; Clifford, S.; Cioslowski, J.; Stefanov, B. B.; Liu, G.; Liashenko, A.; Piskorz, P.; Komaromi, I.; Martin, R. L.; Fox, D. J.; Keith, T.; Al-Laham, M. A.; Peng, C. Y.; Nanayakkara, A.; Challacombe, M.; Gill, P. M. W.; Johnson, B.; Chen, W.; Wong, M. W.; Gonzalez, C.; Pople, J. A. *Gaussian 03*, Revision C.02; Gaussian, Inc.: Pittsburgh, PA, 2004.

(18) (a) Becke, A. D. *Phys. Rev. A: At., Mol., Opt. Phys.* **1988**, *38*, 3098. (b) Perdew, J. P.; Burke, K.; Wang, Y. *Phys. Rev. B: Condens. Matter Mater. Phys.* **1996**, *54*, 16533.

(19) Dolg, M.; Stoll, H.; Preuss, H.; Pitzer, R. M. *J. Phys. Chem.* **1993**, *97*, 5852.

(20) Huzinaga, S.; Anzelm, J.; Klobukowski, M.; Radzio-Andzelm, E.; Sakai, Y.; Tatewaki H. *Gaussian Basis Sets for Molecular Calculations*; Elsevier: Amsterdam, 1984.

(21) (a) Miertus, S.; Scrocco, E.; Tomasi, J. *Chem. Phys.* **1981**, *55*, 117. (b) Miertus, S.; Tomasi, J. *Chem. Phys.* **1982**, *65*, 239. (c) Cossi, M.; Barone, V.; Cammi, R.; Tomasi, J. *Chem. Phys. Lett.* **1996**, *255*, 327. (d) Cossi, M.; Scalmani, G.; Rega, N.; Barone, V. *J. Chem. Phys.* **2002**, *117*, 43.

(22) Bondi, A. *J. Phys. Chem.* **1964**, *68*, 441.

(23) (a) Gonzalez, C.; Schlegel, H. B. *J. Chem. Phys.* **1989**, *90*, 2154. (b) Gonzalez, C.; Schlegel, H. B. *J. Phys. Chem.* **1990**, *94*, 5523.

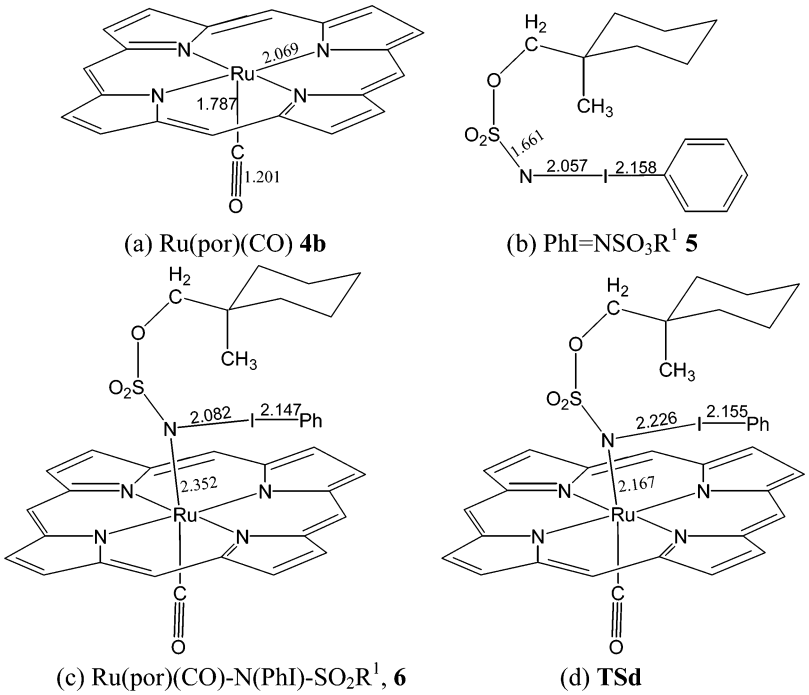

FIGURE 1. Simple schematic diagrams of the BPW91/BS1 optimized geometries of the Ru(por)(CO) catalyst (a), iminoiodane, PhI═NSO$_3$R^1 (b), the ruthenium−iminoiodane complex (c), and the transition state (d) of its decomposition to ruthenium−nitrene and PhI. Key distances (in Å) are indicated. Ball-and-stick pictures directly generated from Gaussian data for all the computed structures in this paper are presented in the Supporting Information.

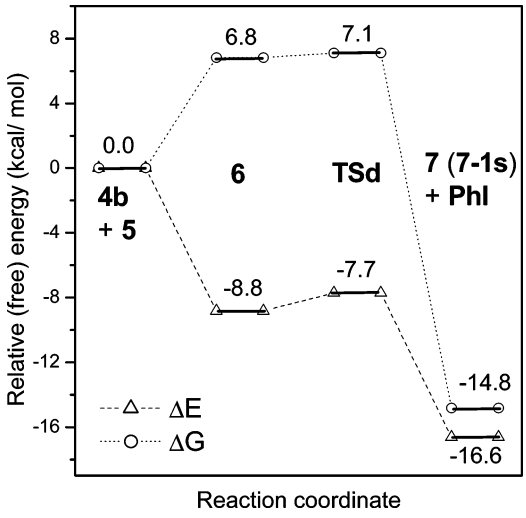

FIGURE 2. Energy (in dashed lines with triangles) and free energy (in dotted line with circles) profiles of the formation of the Ru(por)(CO)−NSO$_3$R^1 complex **7** (the case of **7-1s**) from the starting materials, **4b** + **5**. See Scheme 2 and Figure 1 for details.

optimized geometries of the starting materials, Ru(por)(CO) **4b** and PhI═NSO$_3$R^1 **5**, are depicted in Figure 1a,b. Figure 1c presents the geometry of the metal−iminoiodane complex **6** formed from these two starting materials. The formation of **6** from **4b** + **5** is exothermic by 8.8 kcal/mol (see Figure 2), while the free energy profile depicted in Figure 2 shows that the free energy of **6** is 6.8 kcal/mol higher than that of (**4b** + **5**. This is different from that of a similar reaction catalyzed by Rh$_2$(O$_2$CH)$_4$,[16] in that the stabilization energy (ΔE) for the Rh$_2$(O$_2$CH)$_4$−iminoiodane formation from the staring materials was around 20 kcal/mol, and ΔG also favors this process by about 8 kcal/mol. The large difference of ΔE and ΔG of **6** relative to the starting materials (**4b** + **5**) is a consequence of entropy loss. The subsequent decomposition of **6** to form the metal−nitrene complex, Ru(por)(CO)−NSO$_3$R^1 **7**, accompanied by the release of iodobenzene (PhI) is favorable in free energy by 21.9 kcal/mol. A transition state structure was located for the PhI detachment (**TSd**, Figure 1d). The geometry of **TSd** differs with that of **6** slightly, in that the Ru−N bond length decreases from 2.352 Å in **6** to 2.167 Å in **TSd**, and the N−I bond length increases from 2.082 to 2.226 Å. This implies that the decomposition process of **6** takes place very easily, which is verified in Figure 6 that shows that the free energy of activation is only 0.3 kcal/mol for the **6** → **7** + PhI step. The computed structure of **7** is depicted in Figure 3. As compared to the staring materials (**4** + **5b**), the formation of **7** is favored by 14.8 kcal/mol in free energy, revealing that it can be easily generated in the reaction system.

It should be noted that R^1 contains a cyclohexyl moiety. It is well-documented that a monosubstituted cyclohexane has two chair forms, usually both of which have a similar stability and can be easily changed into each other at room temperature.[24] The two chair forms of Ru(por)(CO)−nitrene complex **7** can be identified by examining the C$^{(4)}$−C$^{(5)}$ bond, which is either equatorial (denoted as **7-1** for chair 1) or axial (**7-2** for chair 2). On the other hand, a metal−nitrene complex may exist in either a singlet or a triplet state. Therefore, **7-1s**, **7-1t** and **7-2s**, **7-2t** are denoted as the singlet and triplet states of the two chair forms of **7** studied in this work, respectively. Figure 3 presents the geometries for **7-1s**, **7-1t**, **7-2s**, and **7-2t**. As they are very close to each other in energy/free energy (see Tables 1 and 2), the energy profile for the **6** → **7** + PhI step was only examined in the case of **7-1s**.

(24) Eliel, E. L.; Allinger, N. L.; Angyal, S. J.; Morrison, G. A. *Conformational Analysis*; John Wiley and Sons, Inc.: New York, 1965; Ch. 2, p 36.

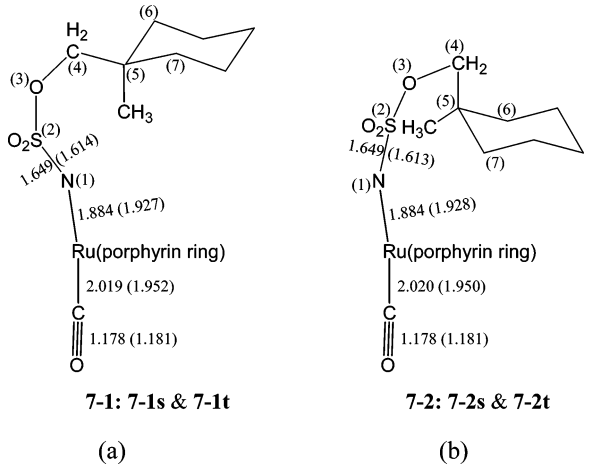

FIGURE 3. Simple schematic diagrams of the BPW91/BS1 optimized geometries obtained for singlet and triplet states of the Ru(por)(CO)−NSO_3R^1 complex **7**, with the cyclohexane moiety in chair 1 (**7-1**, including **7-1s** and **7-1t**, **s** for singlet and **t** for triplet) and chair 2 (**7-2**, including **7-2s** and **7-2t**) conformations. Key distances (in Å) are indicated. The $C^{(4)}-C^{(5)}$ bond is equatorial for chair 1 and axial for chair 2. The parameters for the **7-1t** and **7-2t** triplet states are shown in parentheses.

TABLE 2. Thermodynamic Data (kcal/mol) with Reference of 7-1s for All Reactants, Transition States, and Product Complexes Computed for the Twelve Pathways of C−H Bond Amidation

structure	E + ZPE	ΔG (gas)	ΔG (sol)	structure	E + ZPE	ΔG (gas)
7-1s	0.0	0.0	0.0			
7-1t	0.8	−0.3	−0.1			
7-2s	−0.2	−0.8	0.0			
7-2t	0.7	−1.1	−0.6			
TSi-s	19.7	22.8	20.4	**P**Ci-s	−36.6	−38.4
TSii-s	11.3	14.7	13.4	**P**Cii-s	−40.6	−41.6
TSiii-s	12.2	15.5	13.3	**P**Ciii-s	−41.6	−40.0
TSiv-s	16.3	19.2	17.4	**P**Civ-s	−41.2	−39.3
TSv-s	9.0	12.3	12.1	**P**Cv-s	−41.0	−37.7
TSvi-s	11.6	14.6	13.6	**P**Cvi-s	−36.4	−33.1
TSi-t	18.9	20.1	20.6	**P**Ci-t	6.8	4.1
TSii-t	14.9	16.6	16.9	**P**Cii-t	8.8	9.0
TSiii-t	20.1	22.0	22.8	**P**Ciii-t	7.3	5.5
TSiv-t	18.1	20.0	20.5	**P**Civ-t	4.9	7.5
TSv-t	12.2	13.8	14.8	**P**Cv-t	7.7	8.0
TSvi-t	14.7	15.9	16.6	**P**Cvi-t	7.1	5.0

3.2. Energy Difference between Singlet and Triplet States of Ru(por)(CO)−NSO_3R^1. The energy difference between singlet and triplet states ($E_{st} = E_{singlet} - E_{triplet}$) is often an issue of discussion in nitrene chemistry.[25] In our previous work,[16] it was found that the pure Becke's exchange functional in conjunction with the PW91 or LYP correlation functionals was appropriate for describing the E_{st} of $Rh_2(O_2CH)_4$−NH. In this work, BPW91 functionals were used for the geometry optimization and energy calculation. Although Ru(por)(CO) was used to model the Ru(F_{20}-TPP)(CO) species, there are still 67 atoms for Ru(por)(CO)−NSO_3R^1 and even more atoms for the Ru(por)(CO)−iminoiodane complex. Thus, it is important to find an appropriate basis set for the description of the E_{st} of Ru(por)(CO)−NSO_3R^1, as well as the energy barrier of its C−H bond amidation reactions. Figure 3a shows the BPW91/BS1 optimized geometries of **7-1s** and **7-1t**. The E_{st} values of **7-1** ($E_{7-1s} - E_{7-1t}$) computed with different basis set levels and with the consideration of the solvation effect are listed in Table 1. It was found that the E_{st} values were close to zero in all of the basis set levels used here (e.g., BS1 to ∼BS3), revealing that the BPW91/BS1 level of theory is appropriate for describing the energy difference of the singlet and triplet states of the ruthenium−nitrene complex **7**.

In our previous work,[16] we demonstrated that the small E_{st} value can be attributed to the $\pi-\pi$ interactions between the N and the metal atoms. The Ru−N bonding of the ruthenium−nitrene complex in its singlet and triplet states is illustrated in Figure 4a,b, respectively. For a free nitrene (N−X), the two π' (a prime symbol is used to denoted the free nitrene orbitals) orbitals are degenerate if X is not a π orbital donor. Four electrons occupy one σ'_{N-X} orbital and one lone pair σ' orbital, two doubly degenerate π' orbitals are both singly occupied, and one antibonding $\sigma^{*\prime}_{N-X}$ is unoccupied. As these two degenerate π' orbitals are frontier orbitals, and according to Hund's principle, the two π' orbitals should be both singly occupied; this leads to a triplet state being the ground state. A singlet nitrene is energetically unstable for an additional paired energy (E_p) that is needed as compared to a triplet nitrene, by the equation $E_{st} = E_p$. However, the frontier orbitals are no longer degenerate when the nitrene nitrogen atom is bonded to the Ru atom. The Ru atom in the Ru(por)(CO) catalyst has a square-based pyramidal ML_5 structure. According to ligand field theory, the five Ru 4d orbitals would be split into three degenerate nonbonding orbitals (d_{xy}, d_{yz}, d_{xz}), one weak antibonding (d_{z^2}), and one strong antibonding ($d_{x^2-y^2}$) orbital, as indicated in Figure 4a,b. For the Ru(por)(CO)−NSO_3R^1 complex, one N−Ru σ bonding and its corresponding antibonding (σ^*) orbital can be constructed from the Ru d_{z^2} orbital and the nitrene σ' orbital. Two N−Ru π bonding (1π and 2π) orbitals and their corresponding π^* antibonding orbitals ($1\pi^*$ and $2\pi^*$) can be constructed from the two Ru d orbitals (d_{xz} and d_{yz}) and the two nitrene π' orbitals, respectively. As there are 10 electrons residing in the Ru−N orbitals, the frontier orbitals (i.e., HOMO and LUMO for the singlet Ru(por)(CO)−nitrene or two singly occupied molecular orbitals (SOMOs) for the triplet Ru(por)(CO)−nitrene) are $1\pi^*$ and $2\pi^*$. Although d_{xz} and d_{yz} are degenerate, and at the same time, the two nitrene π' orbitals are degenerate, the $1\pi^*$ and $2\pi^*$ orbitals are no longer degenerate. This is because the lobes of the d_{xz} and d_{yz} orbitals are vertical to each other, while the lobes of the two nitrene π' orbitals are not vertical to each other, considering that the Ru−$N^{(1)}-S^{(2)}$ angle is 125° in **7-1s** and around 140° in **7-1t**. The $1\pi^*$ and $2\pi^*$ antibonding orbitals can be identified by the visualized Kohn−Sham[26] frontier orbitals of **7-1s** and **7-1t**. The HOMO and LUMO of **7-1s** are depicted in Figure 5a,b, and the two SOMOs (with the order $E_{SOMO1} < E_{SOMO2}$) of **7-1t** are depicted in Figure 5c,d. Figure 5 shows that LUMO/SOMO2 has a larger contribution of the nitrene π' orbital than HOMO/SOMO1, which was supported by an examination of the molecular orbital coefficient of the N 2p basis in these frontier orbitals. Because the frontier orbitals are no longer degenerate, the energy split (E_Δ) of the frontier orbitals favors the singlet over the triplet state of the metal−nitrene complexes by $E_{st} = E_p - E_\Delta$, which accounts for the small E_{st} value found in Ru(por)(CO)−NSO_3R^1. As a consequence, the C−H amidation step

(25) Gritsan, N. P.; Platz, M. S.; Borden, W. T. In *Computational Methods in Photochemistry*; Kutateladze, A. G., Ed.; Taylor and Francis: New York, 2005; Vol. 13, Ch. 5, p 235.

(26) Kohn, W.; Sham, J. L. *Phys. Rev. A: At., Mol., Opt. Phys.* **1965**, *140*, 1133.

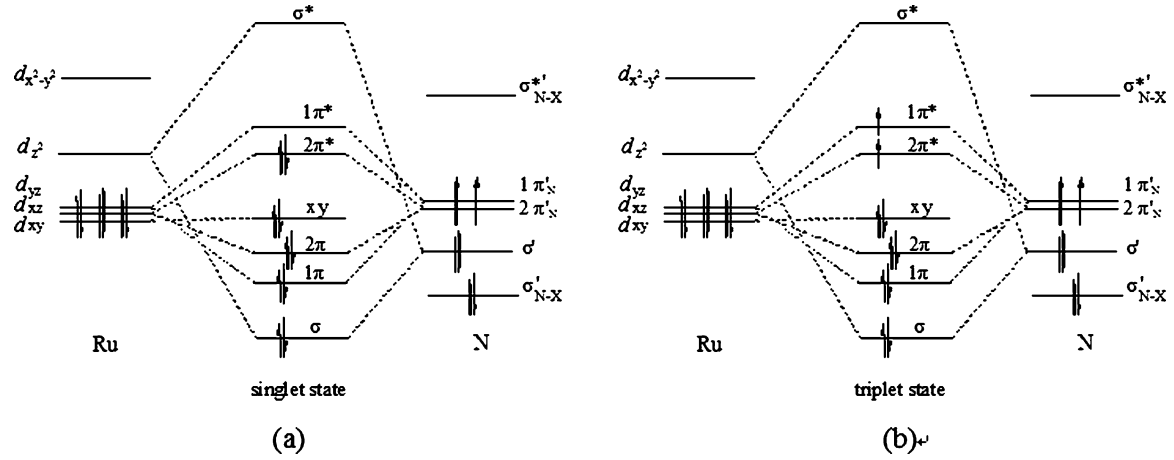

FIGURE 4. Schematic diagrams of the valence electron configuration of the Ru−N bonding in the singlet (a) and triplet (b) states of the Ru(por)(CO)−NSO_3R^1 complex.

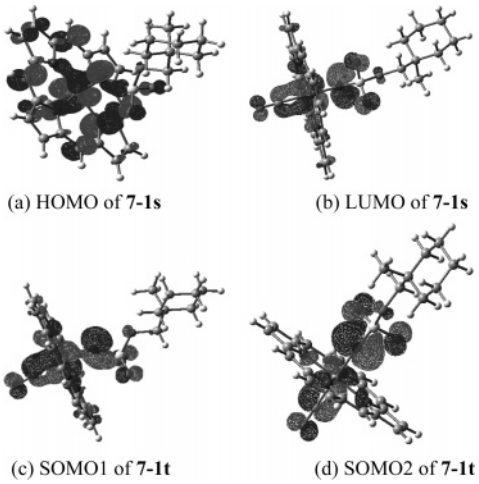

FIGURE 5. Schematic diagrams of the Kohn−Sham frontier orbitals for **7-1s** and **7-1t**. Isovalue: 0.04.

starting from Ru(por)(CO)−NSO_3R^1 **7** should be examined on both singlet and triplet PES.

3.3. Six C−H Bond Amidation Pathways on Both Singlet and Triplet PES. To probe the C−H bond amidation step from Ru(por)(CO)−NSO_3R^1 **7**, it is important to examine the possible reaction pathways that produce a six-membered ring amide **3** by conformational analysis of **7**. As mentioned in section 3.1., two chair forms of **7** can be identified by examination of the $C^{(4)}$−$C^{(5)}$ bond. These two chair forms are either equatorial (**7-1** for chair 1 in Scheme 3) or axial (**7-2** for chair 2). Table 2 shows that **7-2** is only slightly lower in energy than **7-1**. As illustrated in Scheme 3, for **7-1**, there are four C−H bond amidation pathways that lead to four different diastereomers of the six-membered ring amide **3**. These four pathways are (i) amidation of the axial $C^{(6)}$−H bond leading to the (5*R*, 6*S*) diastereomer, (ii) amidation of the equatorial $C^{(6)}$−H bond leading to the (5*R*, 6*R*) diastereomer, (iii) amidation of the axial $C^{(7)}$−H bond leading to the (5*S*, 7*R*) diastereomer, and (iv) amidation of the equatorial $C^{(7)}$−H bond leading to the (5*S*, 7*S*) diastereomer. For **7-2**, only two C−H bond amidation pathways were examined: (v) amidation of the equatorial $C^{(6)}$−H bond leading to the (5*R*, 6*S*) diastereomer and (vi) amidation of the equatorial $C^{(7)}$−H bond leading to the (5*S*, 7*R*) diastereomer. We did not find the transition states and product complexes from **7-2** for the formation of the two trans diastereomers, (5*R*, 6*R*) and (5*S*, 7*S*). It seems unreasonable to construct a six-membered ring amide, in which the dihedral angle of $C^{(4)}$−$C^{(5)}$−$C^{(6)}$−$N^{(1)}$ or $C^{(4)}$−$C^{(5)}$−$C^{(7)}$−$N^{(1)}$ is ∼180°.

Table 2 also shows that the singlet−triplet free energy difference of **7** in both the chair forms is only 0.3 kcal/mol, with the triplet states having slightly lower free energies. As a consequence, all of the six C−H bond amidation pathways described in Scheme 3 may undergo reaction on both singlet and triplet PESs. In the following text, **TS*n*-s** and **TS*n*-t** (*n* = i, ..., vi) denote, respectively, the singlet and triplet transition state with the *n*th C−H bond amidation pathway. **PC*n*-s** and **PC*n*-t** denote the product complex reached via the respective **TS*n*-s** and **TS*n*-t** (see Scheme 2 for notations). Figure 6 depicts all of the geometries for all of the transition states and product complexes located for the six pathways on the singlet PES. Figure 7 depicts those on the triplet PES. The free energy profiles for each of the 12 C−H bond amidation pathways are depicted in Figure 8. The energy and free energy of each optimized structure involved in these 12 reaction pathways are collected in Table 2.

Inspection of Figure 6 reveals that each **TS*n*-s** has a trigonal C···H···N geometry, in which the H atom detaches from the C atom and approaches the N atom. This is similar to the results of the $Rh_2(O_2CH)_4$-catalyzed C−H bond amidations and results reported by Nakamura et al. for the $Rh_2(COOH)_4$-catalyzed C−C bond formation reactions.[27] For example, in **TSi-s** (see the first panel of Figure 6) that is proceeded by **7-1s**, the H atom in the axial $C^{(6)}$−H bond detaches from $C^{(6)}$ with a $C^{(6)}$···H distance of 1.394 Å and approaches $N^{(1)}$ with a $N^{(1)}$···H distance of 1.259 Å. In the product complexes **PCi-s** that are proceeded by **TSi-s**, both C−N and N−H bonds are formed. It was found that **PCi-s** is the van der Waals complex between the catalyst (**4b**) and the six-membered ring amide **3**, in the (5*R*, 6*S*) configuration, since the $N^{(1)}$ atom completely detaches from the Ru atom as can be identified from the N···Ru distance being larger than 4 Å. This is different from the case of the Rh(II)-catalyzed C−H bond amidation, where the amide product is still bonded to the Rh atom after the C−N bond formation, although the decomposition of the amide product from the catalyst is facile. The free energy of activation of the **7-1s** →

(27) Nakamura, E.; Yoshikai, N.; Yamanaka, M. *J. Am. Chem. Soc.* **2002**, *124*, 7181.

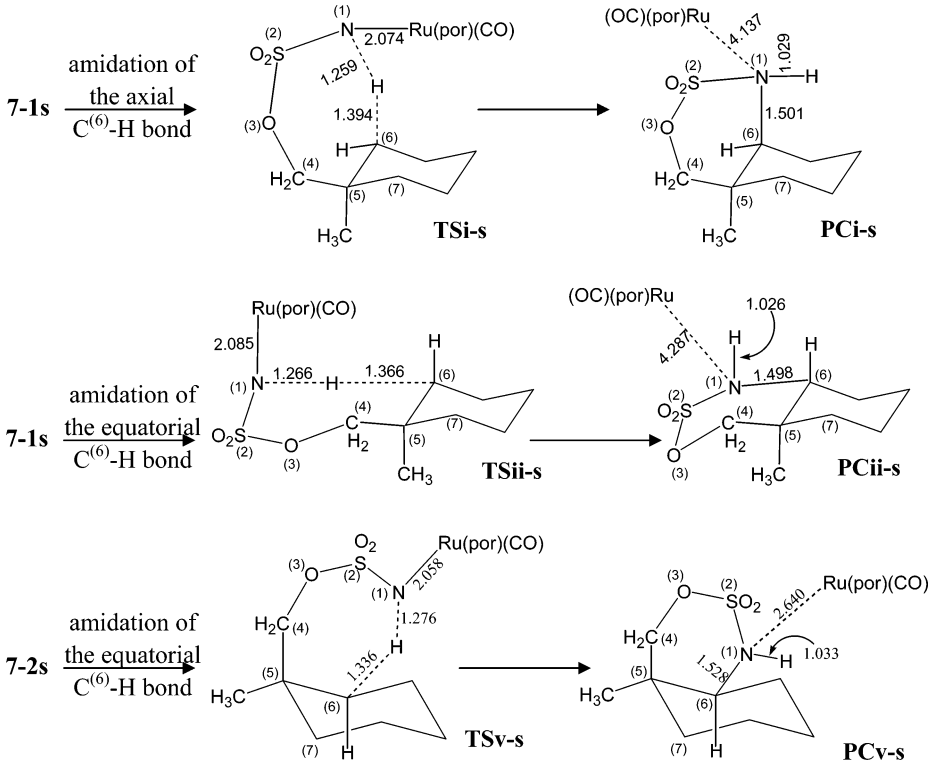

FIGURE 6. Simple schematic diagrams of the BPW91/BS1 optimized geometries of (**TS*n*-s**) and (**PC*n*-s**), where n = i to ∼vi (structures for n = i, ii, and v are presented here and for n = iii, iv, vi are in the Supporting Information), respectively. Key distances (in Å) are indicated. See Scheme 3 and text for details.

SCHEME 3. Six Reaction Pathways of Nitrene Insertion into a C−H Bond to Form a Six-Membered Ring Amide Product via Two Chair Forms of 7 (7-1 and 7-2) in Both Singlet and Triplet States

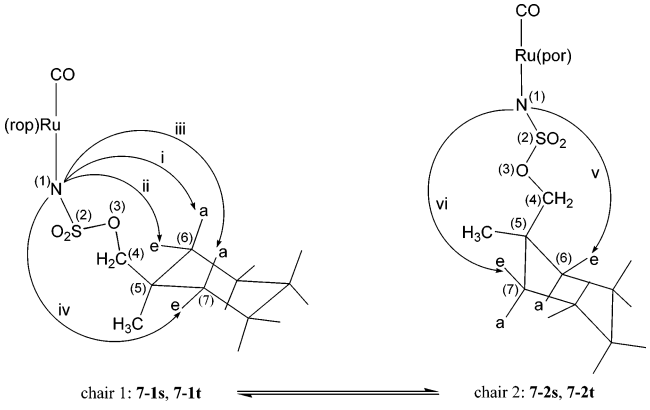

TSi-s → **PCi-s** pathway is 22.8 kcal/mol, and the free energy change of it goes downhill with a decrease of 38.4 kcal/mol. Table 1 depicts the energy of activation for this pathway with different basis set levels and with the consideration of the solvation effect. The calculation results show that BPW91/BS1 is also appropriate for characterization of the energy profile of the C−H bond amidation step.

In **TSii-s** that is preceded by **7-1s**, the H atom in the equatorial $C^{(6)}$−H bond detaches from $C^{(6)}$ with a $C^{(6)}$···H distance of 1.366 Å and approaches the N atom with a N···H distance of 1.266 Å. Amide **3** in the (5*R*, 6*R*) diastereomer can be identified in **PCii-s** that is preceded by **TSii-s**. In **TSiii-s** preceded by **7-1s**, the H atom in the axial $C^{(7)}$−H bond detaches from $C^{(7)}$ with a $C^{(7)}$···H distance of 1.384 Å and approaches the N atom with a N···H distance of 1.261 Å. Amide **3** in the (5*S*, 7*R*) diastereomer can be identified in **PCiii-s** preceded by **TSiii-s**. In **TSiv-s** that is preceded by **7-1s**, the H atom in the equatorial $C^{(7)}$−H bond detaches from $C^{(7)}$ with a $C^{(7)}$···H distance of 1.386 Å and approaches the N atom with a N···H distance of 1.247 Å. Amide **3** in the (5*S*, 7*S*) diastereomer can be identified in **PCiv-s** that is preceded by **TSiv-s**.

In **TSv-s** that is preceded by **7-2s**, the H atom in the equatorial $C^{(6)}$−H bond detaches from $C^{(6)}$ with a $C^{(6)}$ ···H distance of 1.336 Å and approaches the N atom with a N···H distance of 1.276 Å. Amide **3** in the (5*R*, 6*S*) configuration can be identified in **PCv-s** that is preceded by **TSv-s**. In **TSvi-s** that is preceded by **7-2s**, the H atom in the equatorial $C^{(7)}$−H bond detaches from $C^{(7)}$ with a $C^{(7)}$···H distance of 1.339 Å and approaches the N atom with a N···H distance of 1.259 Å. Amide **3** in the (5*S*, 7*R*) configuration can be identified in **PCvi-s** that is preceded by **TSvi-s**. Further inspection of the geometrical parameters of the C···H and N···H distances in each **TS*n*-s** revealed that the C···H distances in the six transition state structures follow the following order: **TSv-s** < **TSvi-s** < **TSii-s** < **TSiii-s** < **TSiv-s** < **TSi-s**, and the N···H distances roughly follow the reverse order. This suggests that the order of the free energy of activation for these six pathways may follow **v** < **vi** < **ii** < **iii** < **iv** < **i** on the singlet PES, which is supported by the results given in Figure 8 and Table 2.

Inspection of Figure 7 shows that each **TS*n*-t** also has a trigonal C···H···N geometry. For example, in **TSv-t** (see Figure 7) that is preceded by **7-2t**, the H atom in the axial $C^{(6)}$−H bond detaches from $C^{(6)}$ with a $C^{(6)}$···H distance of 1.387 Å and approaches $N^{(1)}$ with a $N^{(1)}$···H distance of 1.271 Å. The $C^{(6)}$···H distance in **TSv-t** is longer than that in **TSv-s**, and the $N^{(1)}$···H distance is shorter. This suggests that C−H bond

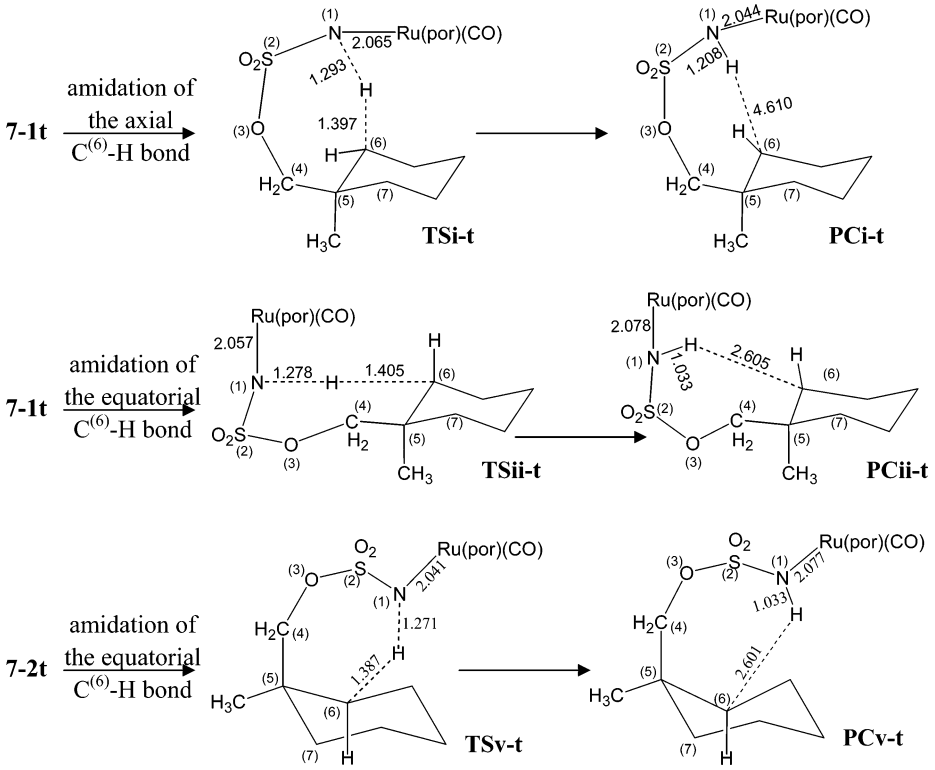

FIGURE 7. Simple schematic diagrams of the BPW91/BS1 optimized geometries of (**TS*n*-t**) and (**PC*n*-t**), where n = i to ∼vi (structures for n = i, ii, v are presented here and for n = iii, iv, vi are in the Supporting Information), respectively. Key distances (in Å) are indicated. See Scheme 3 and text for details.

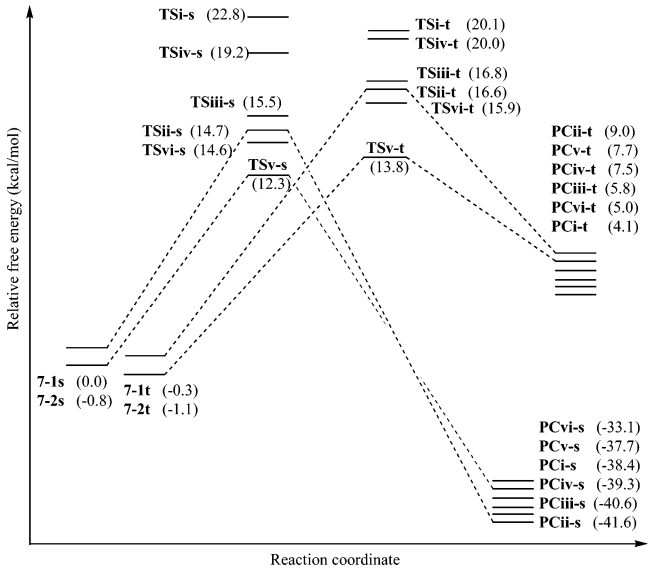

FIGURE 8. Free energy profiles of the six C−H bond amidation pathways of the Ru(por)(CO)−NSO_3R^1 complex on both singlet and triplet PES. See Schemes 1 and 3, Figures 6 and 7, Table 2, and the text for details.

amidation on the triplet PES may be more difficult than that on the singlet PES for pathway v (see Scheme 3), which is supported by the observation in Figure 8 that **TSv-t** is 1.5 kcal/mol higher in free energy than that of **TSv-s**. The geometry of each **PC*n*-t** has a dramatic difference from that for each **PC*n*-s**, in that in the former, the C−N bond does not form, and the N−Ru bond does not cleave. For example, in **PCv-t**, the $N^{(1)}$−H bond was formed with a bond length of 1.033 Å, while the $C^{(6)}$···H distance was 2.601 Å, and the $C^{(6)}$···N distance was 3.505 Å. Similar cases were found for the other **PC*n*-t** structures. The spin densities of the $N^{(1)}$ atoms and the $C^{(6)}$/$C^{(7)}$ atoms in each of the **PC*n*-t** indicates that they are all biradicals, with two unpaired electrons residing on the $N^{(1)}$ atom and $C^{(6)}$/$C^{(7)}$ atoms. For example, for the fifth triplet reaction pathway, the spin densities of the selected atoms are collected in Table 3. The spin density of the N + Ru + (por)(CO) portion of the molecule was 1.744 (two unpaired electrons), indicating that it was a triplet state of metal−nitrene character. This value decreases to 1.683 in **TSv-s** and to 0.983 in **PCv-s**. The spin density of the $C^{(6)}$ atom is zero (no unpaired electron) in **7-2t** and increases to 0.536 in **TSv-s** and 1.008 in **PCv-s**. These results show that one electron transfers from the N atom to the $C^{(6)}$ atom in the **7-2t** → **TSv-t** → **PCv-t** process and that **PCv-t** is a biradical. Since a biradical may undergo recombination easily, it is reasonable to expect that each **PC*n*-t** could easily turn into its corresponding **PC*n*-s** through C−N bond formation, which is an intramolecular biradical recombination process. As a result, a certain C−H bond amidation pathway that undergoes reaction on both singlet and triplet PESs may finally lead to the same product, and this is indicated in Scheme 1.

TABLE 3. Spin Densities of Selected Atoms and Groups in 7-2t, TSv-t, and PCv-t, Respectively

atom/group	**7**-2t	**TS**v-t	**PC**v-t
Ru	0.504	0.349	0.337
N	0.898	0.667	0.281
(por)(CO)	0.372	0.267	0.320
SO_3	0.221	0.147	0.077
$C^{(6)}$	0.000	0.536	1.008

3.4. Prediction of the Diastereoselectivity of the Amidation Product. As depicted in both Figure 8 and Table 2, the reaction

TABLE 4. Rate Constants for Each Reaction Pathway Relative to That of the Fifth Singlet Pathway (k_i/k_{v-s}) Computed in the Gas-Phase and DPCM/BONDI Solvation Models

reaction pathways	configuration of amide **3** produced	k_i/k_v-s (gas)	k_i/k_v-s (DPCM/BONDI)
7-1s → TSi-s → PCi-s	(5*R*, 6*S*)	4.4×10^{-8}	3.1×10^{-7}
7-1s → Tsii-s → PCii-s	(5*R*, 6*R*)	2.1×10^{-2}	0.12
7-1s → TSiii-s → PCiii-s	(5*S*, 7*R*)	5.5×10^{-3}	3.1×10^{-2}
7-1s → TSiv-s → PCiv-s	(5*S*, 7*S*)	1.5×10^{-5}	1.6×10^{-4}
7-2s → TSv-s → PCv-s	(5*R*, 6*S*)	1.0	1.0
7-2s → TSvi-s → PCvi-s	(5*S*, 7*R*)	2.4×10^{-2}	8.7×10^{-2}
7-1t → TSi-t → PCi-t	(5*R*, 6*S*)	3.8×10^{-6}	1.3×10^{-6}
7-1t → TSii-t → PCii-t	(5*R*, 6*R*)	9.3×10^{-4}	4.5×10^{-4}
7-1t → TSiii-t → PCiii-t	(5*S*, 7*R*)	1.6×10^{-7}	3.3×10^{-8}
7-1t → TSiv-t → PCiv-t	(5*S*, 7*S*)	4.1×10^{-6}	1.3×10^{-6}
7-2t → TSv-t → PCv-t	(5*R*, 6*S*)	8.2×10^{-2}	1.2×10^{-2}
7-2t → TSvi-t → PCvi-t	(5*S*, 7*R*)	3.2×10^{-3}	8.2×10^{-4}

barrier of the pathway **7-2s → TSv-s → PCv-s** is the lowest among those of the 12 C−H bond amidation pathways (see Scheme 3) examined in this work, and the reaction barrier for **7-2t → TSv-t → PCv-t** is the lowest among the six C−H bond amidation pathways on the triplet PES. Both of these two pathways lead to amide product **3** as a (5*R*, 6*S*) diastereomer as indicated in Scheme 3. It is essential to calculate the relative reaction rates of these 12 C−H bond amidation pathways to predict the overall diastereoselectivity of this reaction. Inclusion of the bulk CH_2Cl_2 solvation effect was examined by additional PCM calculations. Since all of the **TS**s involves a H atom transfer from the C atom to the N atom, BONDI atomic radii were used in the D-PCM calculations, in which the H atoms were explicitly considered to build up the solvation cavity. Table 4 lists the rate constant for each pathway relative to that of pathway **7-2s → TSv-s** (i.e., k_i/k_{v-s} calculated by using transition state theory),[28] in both the gas-phase model and the DPCM/BONDI solution model.

The DPCM results listed in Tables 2 and 4 suggest that the singlet pathways are favored over the triplet pathways when the solvation effect is considered. For example, k_{v-t}/k_{v-s} is 0.012 in the solution phase, while this value is only 0.082 in the gas phase. This is consistent with the results of the $Rh_2(O_2CH)_4$-catalyzed C−H bond amidation reaction.[16] The results reported in ref 16 showed that the singlet pathway involves a hydride transfer accompanied by a large charge transfer from the C atom to the N atom, while in the triplet pathways, the C−H bond undergoes homolytic cleavage, accompanied by a H atom transfer to the N atom to form a biradical, which suggests that the solvation effect favors a process that has a large charge-transfer character. The nitrene insertion into the C−H bond step is first order, and the relative reaction rate of producing the four diastereomers can be obtained from the following equations:

$$r_i = k_i C(\mathbf{7})$$

and

$$r_{5R,6S}:r_{5R,6R}:r_{5R,7S}:r_{5S,7S} = (k_{i-s} + k_{i-t} + k_{v-s} + k_{v-t}):(k_{ii-s} + k_{ii-t}):(k_{iii-s} + k_{iii-t} + k_{vi-s} + k_{vi-t}):(k_{iv-s} + k_{iv-t})'$$

where $C(\mathbf{7})$ is the concentration of the metal−nitrene complex **7**. Using the rate constant data listed in Table 4, $r_{5R,6S}:r_{5R,6R}:r_{5S,7R}:r_{5S,7S}$ can be easily calculated to be $1:0.019:0.003:1.8 \times 10^{-6}$ in the gas-phase model and $1:0.12:0.12:1.6 \times 10^{-4}$ in the DPCM model, that is, around 98% (gas-phase model) or 81% (DPCM) of the amidation product **3** is in the (5*R*, 6*S*) configuration. This is in good agreement with the results reported in ref 8g.

4. Conclusion

In summary, a complete catalytic cycle of Ru-catalyzed intramolecular C−H bond amidation of a sulfamate was characterized by DFT computations and used to predict the stereoselectivity of this reaction. A metal−nitrene complex, Ru(por)(CO)−NSO_3R^1, which can be easily generated from the iminoiodane, is directly responsible for the nitrene insertion step of the reaction mechanism. In the 12 C−H bond amidation pathways that generate a six-membered ring amide **3**, the pathway indicated as **7-2s → TSv-s → PCv-s** in Scheme 3 on the singlet PES is predicted to be the most efficient, and **7-2t → TSv-t → PCv-t** is predicted to be the most efficient among the triplet pathways. These two reaction pathways both lead to the **3** (5*R*, 6*S*) diastereomer amidation product, which is consistent with experimental results reported in ref 8g. This study contributes to a better understanding of the reaction mechanisms, as well as provides some insight into predicting the stereoselectivity of metal-catalyzed C−N bond formation reactions.

Acknowledgment. This research was supported by grants from the Research Grants Council of Hong Kong HKU 7011/04P to C.-M.C. and HKU/7021/03P to D.L.P. and the Area of Excellence Scheme established under the University Grants Committee of the Hong Kong Special Administrative Region, China (AoE/P-10/01) to C.-M.C.

Supporting Information Available: Compound structures both in ball-and-stick model and in simple schematic diagram, Cartesian coordinates of optimized geometries, calculated zero-point corrected energies, and free energies at 313.15 K (in hartrees) for all compounds depicted. This material is available free of charge via the Internet at http://pubs.acs.org.

JO702011Z

(28) (a) Kreevoy, M. M.; Truhlar, D. G. Investigation of Rates and Mechanisms of Reaction. In *Techniques of Chemistry*, 4th ed.; Bernasconi, C. F., Ed.; John Wiley and Sons; New York, 1986; Vol. 6, p 13. (b) It can be easily deduced that $k_i/k_{v-s} = \exp[(G_{TSi} - G_{TSv-s})/RT]$, where R is the universal gas constant and T is the temperature.